

Electron-Ion Recombination Rate Coefficients and Photoionization Cross Sections for Astrophysically Abundant Elements. IX. Ni XXVI and Ni XXVII for UV and X-ray modeling

Sultana N. Nahar

Department of Astronomy, The Ohio State University, Columbus, OH 43210

nahar@astronomy.ohio-state.edu

ABSTRACT

The inverse processes of photoionization and electron-ion recombination of ($h\nu + \text{Ni XXVI} \leftrightarrow \text{Ni XXVII} + e$) and ($h\nu + \text{Ni XXVII} \leftrightarrow \text{Ni XXVIII} + e$) are studied using the unified method for the total recombination. The method subsumes both the radiative and di-electronic recombination processes and enables self-consistent sets of results for photoionization and electron-ion recombination by using the same wavefunction for these inverse processes. Photoionization cross sections (σ_{PI}), recombination cross sections (σ_{RC}), recombination collision strengths (Ω_{RC}), and recombination rate coefficients (α_{RC}) are obtained for ionization balance and spectral analysis of UV and X-ray lines. Level-specific photoionization cross sections and recombination rates are presented to enable accurate computation of recombination-cascade matrices for all fine structure levels n (ℓ SLJ) up to $n \leq 10$: 98 bound fine structure levels of Ni XXVI with $0 \leq l \leq 9$, $0 \leq L \leq 11$, $1/2 \leq J \leq 17/2$, and 198 levels of Ni XXVII with $0 \leq l \leq 9$, $0 \leq L \leq 14$, $0 \leq J \leq 10$. Total α_{RC} for Ni XXVI and Ni XXVII are compared with the existing values with very good agreement. Total recombination rate coefficients for the hydrogen-like recombined ion, Ni XXVIII, are also presented. The calculations are carried out in relativistic Breit-Pauli R-matrix (BPRM) approximation with inclusion of radiation damping of resonances. With consideration of all details of the processes, the results, which include the level specific σ_{PI} and α_R calculated for the first time, should be the most accurate for these ions.

Subject headings: atomic data — atomic processes — photoionization, radiative and dielectronic recombination, unified electron-ion recombination — UV and X-rays: general — line formation, ions - Ni XXVI, Ni XXVII, Ni XXVIII

1. INTRODUCTION

From a study of photoionization and electron-ion recombination for Li- and He-like ions, similar to the earlier ones for C IV and C V (Nahar et al. 2000), O VI, O VII (Nahar and Pradhan 2003), Fe XXV and Fe XXV (Nahar et al. 2001), results of cross sections and rates are presented for Ni XXVI and Ni XXVII. These inverse atomic processes of Li-like and He-like ions are of particular interest in the X-ray astronomy for analysis of new observations by space based observatories such as the Chandra X-ray Observatory and XMM-Newton, at photon energies and temperatures prevalent in high-temperature sources such as AGN, supernova remnants, hot stellar coronae etc. (e.g. Canizares et al. 2000).

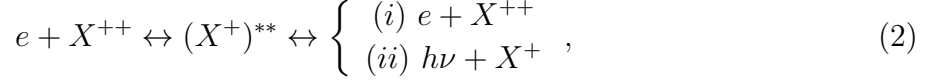
The Li-like and He-like ions show distinctive features, compared to those of higher multi-electron ions, in both photoionization and electron-ion recombination in (i) displaying a featureless smooth structure until at high energies when narrow and dense resonances appear in separated n -complexes, and (ii) the low- n resonances are radiationally damped because of higher radiative decay rates. It is important to consider relativistic fine structure effect explicitly in the theoretical formulation to resolve the narrow resonances and include radiation damping of resonances. Photoionization cross sections, electron-ion recombination cross sections, and rate coefficients are obtained in the unified method for the total electron-ion recombination, accounting both radiative and di-electronic recombination (RR and DR) processes, in the frame of relativistic Breit-Pauli R-matrix (BPRM) method (Nahar & Pradhan 1992, 1994, Nahar 1996, Zhang et al. 1999). The unified method provides a a single set of recombination rate coefficents taking account of both RR and DR in an ab initio manner for the entire temperature range of applications. The aim of the present series of reports (e.g. Nahar and Pradhan 1997) is at studying and presenting accurate atomic parameters for photoionization and total (e+ion) recombination for astrophysical models on a variety of applications.

2. THEORY

The unified method of electron-ion recombination (Nahar & Pradhan 1992, 1994) yields self-consistent sets of atomic parameters for the inverse processes of photoionization and recombination for atoms and ions. Photorecombination of an incident electron with the target ion may occur through (i) non-resonant, background continuum, or radiative recombination (RR),

$$e + X^{++} \leftrightarrow h\nu + X^+, \quad (1)$$

which is the inverse process of direct photoionization, or (ii) through a two-step recombination process via autoionizing resonances, i.e. dielectronic recombination (DR):



The quasi-bound doubly-excited autoionizing state, $(X^+)^{**}$, leads either to (i) autoionization, a radiation-less transition to a lower target state with the electron going into a continuum, or (ii) radiative stabilization to a recombined bound state via radiative decay of the ion core, usually to the ground state, with the capture of the electron.

The unified method subsumes both the RR and DR processes. It considers photoionization from and recombination into the infinity of levels of the $(e + \text{ion})$ system. These recombined levels are divided into two groups: group (A) bound levels with $n \leq n_o$ and all possible fine structure $J\pi$ symmetries, and group (B) levels $n_o < n \leq \infty$; where n_o is the typically 10.

Photoionization and recombination calculations are carried out in detail for all group (A) levels in close coupling (CC) approximation (e.g. Seaton 1997). In the CC approximation the target ion (core) is represented by an N -electron system. The total wavefunction, $\Psi(E)$, of the $(N+1)$ electron-ion system of symmetry $J\pi$ is represented in terms of an expansion of target eigenfunctions as:

$$\Psi(\text{ion} + e; E) = A \sum_i \chi_i(\text{ion}) \theta_i + \sum_j c_j \Phi_j(\text{ion} + e), \quad (3)$$

where χ_i is the target wavefunction for a specific level $J_i\pi_i$ and θ_i is the wavefunction for the $(N+1)$ -th electron in a channel labeled as $S_i L_i(J_i) \pi_i k_i^2 \ell_i(J\pi)$, k_i^2 being its incident kinetic energy. The Φ_j 's are the correlation functions of the $(N+1)$ -electron system that account for short range correlation and the orthogonality between the continuum and the bound orbitals.

In relativistic BPRM calculations, developed under the Iron Project (IP, Hummer et al. 1993), the set of $SL\pi$ are recoupled for $J\pi$ levels of $(e + \text{ion})$ -system, followed by diagonalisation of the Hamiltonian, $H_{N+1}^{\text{BP}} \Psi = E \Psi$, where the BP Hamiltonian is

$$H_{N+1}^{\text{BP}} = H_{N+1}^{\text{NR}} + H_{N+1}^{\text{mass}} + H_{N+1}^{\text{Dar}} + H_{N+1}^{\text{so}}. \quad (4)$$

The first term, H_{N+1}^{NR} , is the nonrelativistic Hamiltonian,

$$H_{N+1}^{\text{NR}} = \sum_{i=1}^{N+1} \left\{ -\nabla_i^2 - \frac{2Z}{r_i} + \sum_{j>i}^{N+1} \frac{2}{r_{ij}} \right\}, \quad (5)$$

and the additional one-body terms are

$$\begin{aligned} &\text{the mass correction term, } H^{\text{mass}} = -\frac{\alpha^2}{4} \sum_i p_i^4, \\ &\text{the Darwin term, } H^{\text{Dar}} = \frac{Z\alpha^2}{4} \sum_i \nabla^2\left(\frac{1}{r_i}\right) \text{ and} \\ &\text{the spin-orbit interaction term, } H^{\text{so}} = Z\alpha^2 \sum_i \frac{1}{r_i^3} \mathbf{l}_i \cdot \mathbf{s}_i, \end{aligned} \quad (6)$$

respectively. The spin-orbit term splits the LS term into fine structure components.

The positive and negative energy states (Eq. 4) define continuum or bound ($e + \text{ion}$) states. $E = k^2 > 0$ for continuum (scattering) channels and $E < 0$ for bound states. The reduced matrix element for the bound-free transition,

$$\langle \Psi_B | |\mathbf{D}| | \Psi_F \rangle, \quad (7)$$

can be obtained from the continuum wavefunction (Ψ_F) and the bound wavefunction (Ψ_B). \mathbf{D} is the dipole operator, $\mathbf{D}_L = \sum_i \mathbf{r}_i$, in length form, the sum is on the number of electrons. The photoionization cross section is obtained as

$$\sigma_{\text{PI}} = \frac{1}{g_i} \frac{4\pi^2}{3c} \omega \mathbf{S}, \quad (8)$$

where g_i is the statistical weight factor of the initial bound state and $\mathbf{S} = |\langle \Psi_B | |\mathbf{D}| | \Psi_F \rangle|^2$ is the dipole line strength. For highly charged H- and the He-like recombining ions, the probability of radiative decay of an autoionizing state is often comparable to that of autoionization (typically $10^{12} - 10^{14} \text{ sec}^{-1}$, as discussed in Nahar et al. 2000). With strong dipole allowed $2p \rightarrow 1s$ and $1s2p ({}^1P_1^o) \rightarrow 1s^2 ({}^1S_0)$ transitions (e.g. Table 2) autoionizing resonances are radiatively damped to a significant extent. The radiative damping effect of all near-threshold resonances, up to effective quantum number $\nu \leq 10$, are considered using a resonance fitting procedure (Sakimoto et al. 1990, Pradhan and Zhang 1997, Zhang et al. 1999).

The photo-recombination cross section, σ_{RC} , is related to photoionization cross section, σ_{PI} , through principle of detailed balance (Milne relation) as

$$\sigma_{\text{RC}}(\epsilon) = \frac{\alpha^2}{4} \frac{g_i}{g_j} \frac{(\epsilon + I)^2}{\epsilon} \sigma_{\text{PI}}. \quad (9)$$

α is the fine structure constant, ϵ is the photoelectron energy, g_j is the statistical weight factor of the recombined ion and I is the ionization potential. σ_{RC} are computed from the photoionization cross sections at a sufficiently large number of energies to delineate the non-resonant background and the autoionizing resonances, thereby representing both radiative and the dielectronic recombination (RR and DR) processes. In the unified treatment the photoionization cross sections, σ_{PI} , of a large number of bound states (group A) – all possible states with $n \leq n_o \sim 10$ – are obtained as described above. It is assumed that the

recombining ion is in the ground state, and recombination can take place into the ground or any of the excited recombined (e+ion) states.

Recombination rate coefficients of individual recombined levels are obtained by convolving recombination cross sections over Maxwellian electron distribution $f(v)$ at a given temperature as,

$$\alpha_{RC}(T) = \int_0^\infty v f(v) \sigma_{RC} dv. \quad (10)$$

Contributions from the low- n group (A) bound levels are added for the total recombination rate coefficient, α_{RC} and for the total recombination cross sections, σ_{RC} .

Group (B) levels, $n_o < n \leq \infty$, are treated through quantum defect theory of DR within close the coupling approximation (Nahar & Pradhan 1992, 1994). A generally valid approximation made in recombination to group (B) levels is that the background contribution is negligible, and DR is the dominant process in the region below the threshold of convergence for high- n resonances. To each excited threshold of the core, $J_i \pi_i$, belongs an infinite series of $(N+1)$ -electron levels, $J_i \pi_i \nu \ell$, to which recombination can occur. For the high ν levels DR dominates while the background RR is small and, hence DR dominates the total recombination. The contributions from these levels are added by calculating the DR collision strengths, Ω_{DR} , an extension (Nahar and Pradhan 1994) of the precise theory of radiation damping by Bell and Seaton (1985):

$$\Omega(DR) = \sum_{SL\pi} \sum_n (1/2)(2S+1)(2L+1) P_n^{SL\pi}. \quad (11)$$

$P_n^{SL\pi}$ is the DR probability in entrance channel n , obtained as $P_n^{SL\pi}(DR) = (\mathbf{1} - \mathcal{S}_{ee}^\dagger \mathcal{S}_{ee})_n$, where \mathcal{S}_{ee} is the matrix for electron scattering *including* radiation damping. The recombination cross section, σ_{RC} in Megabarns (Mb), is related to the collision strength, Ω_{RC} , as

$$\sigma_{RC}(i \rightarrow j)(Mb) = \pi \Omega_{RC}(i, j) / (g_i k_i^2) (a_o^2 / 1. \times 10^{-18}), \quad (12)$$

where k_i^2 is the incident electron energy in Rydbergs. Since σ_{RC} diverges at zero electron energy, the total collision strength, Ω , is used in the recombination rate calculations.

The group (A) levels in the unified method may not be necessarily restricted up to $n = 10$. It can readily be extended to higher n . However, detailed calculations for photoionization cross sections of high- n (> 10) levels is unnecessary since they approach hydrogenic behavior. Background photoionization cross sections for these high- n group (B) levels are computed hydrogenically to contribute to the total recombination rate. This high- n background contribution is referred to as the “high- n top-up” contribution (Nahar 1996).

3. COMPUTATIONS

The calculations for photoionization and electron-ion recombination span several stages of computation starting with obtaining the target (core ion) wavefunction through configuration interaction atomic structure calculations. The wavefunction expansion for Ni XXVI consists of 17 fine structure levels of configurations $1s^2$, $1s2s$, $1s2p$, $1s3s$, $1s3p$, and $1s3d$ of target Ni XXVII. The levels, along with their relative energies, are given in Table 1. The set of correlation configurations in the atomic structure calculations are also given in Table 1. The orbital wavefunctions are obtained from the atomic structure code SUPERSTRUCTURE (Eissner et al. 1974). The Thomas-Fermi scaling parameter (λ_{nl}) for each orbital is taken to be 1. The second term of the wavefunction in Eq. (3), which contains bound state correlation functions for Ni XXVI, includes all possible $(N+1)$ -particle configurations from 0 to maximum orbital occupancies as $2s^2$, $2p^2$, $3s^2$, $3p^2$, $3d^2$, $4s$ and $4p$. The energies in Table 1 are observed values (from the NIST website: www.nist.gov). Radial integrals for the partial wave expansion in Eq. 3 are specified for orbitals $0 \leq \ell \leq 9$, with a R-matrix basis set of 40 ‘continuum’ functions for Ni XXVI. Computations are carried out for all angular momenta, $0 \leq L \leq 11$, $1/2 \leq J \leq 17/2$ for Ni XXVI.

The wavefunction expansion of Ni XXVII consists of 16 fine structure levels of configurations. $1s$, $2s$, $2p$, $3s$, $3p$, $3d$, $4s$, $4p$, $4d$ and $4f$ of Ni XXVIII, as given in Table 1. There are no correlation configurations, and the scaling parameter for each orbital is taken to be unity. The orbital wavefunctions and level energies are obtained from SUPERSTRUCTURE. The energies in Table 1 are the calculated ones. The bound state correlation functions, in the second term of the wavefunction, include all configurations from 0 to maximum orbital occupancies: $1s^2$, $2s^2$, $2p^2$, $3s^2$, $3p^2$, $3d^2$, $4s^2$ and $4p^2$, $4d$ and $4f$. Radial integrals for the partial wave expansion are specified for orbitals $0 \leq \ell \leq 9$, with a R-matrix basis set of 30 ‘continuum’ functions for Ni XXVII. Computations are carried out for all angular momenta, $0 \leq L \leq 14$, $0 \leq J \leq 10$ for Ni XXVII.

Relativistic BPRM calculations in intermediate coupling are carried out in the close coupling approximation using the *R*-matrix package of codes (Berrington et al. 1995). These are extensions of the Opacity Project codes (Berrington et al. 1987) to include relativistic effects (Scott & Burke 1980, Scott & Taylor 1982, Berrington et al. 1995), implemented under the Iron Project (Hummer et al. 1993). The energy levels were identified using code PRCBPID (Nahar and Pradhan 2000).

Both the *partial* and the *total* photoionization cross sections are obtained for all bound levels. Coupled channel calculations for σ_{PI} include both the background and the resonance structures (due to the doubly excited autoionizing states) in the cross sections. Radiation damping of resonances up to $n = 10$ are included through use of the extended codes STGF

and STGBF (Nahar & Pradhan 1994, Zhang et al. 1999). The BPRM calculations are carried out for each total angular momentum symmetry $J\pi$, corresponding to a set of fine structure target levels J_t . Radiation damping of resonances within the close coupling BPRM calculations are described in Zhang et al. (1999, and references therein). The program PBPRAD is used to extend the *total* photoionization cross sections in the high energy region, beyond the highest target threshold in the close coupling wavefunction expansion of the ion, by a ‘tail’ using a fitting formula as well as Kramers formula $\sigma(E) = \sigma_{PI}^o(E^o/E)^3$ where σ^o is the last tabulated cross section at energy E^o above all target thresholds, as described in Nahar and Pradhan (1994).

In the higher energy region, $\nu_o < \nu \leq \infty$, below each target threshold where the resonances are narrow and dense and the background is negligible, we compute detailed and resonance averaged DR cross sections (Bell and Seaton 1985, Nahar and Pradhan 1994). The radiative decay probabilities used for the ions are given in Table 2. The DR collision strengths in BPRM approximation are obtained using extensions of the *R*-matrix asymptotic region code STGF (Nahar & Pradhan 1994, Zhang et al. 1999). It is necessary to use a very fine energy mesh in order to delineate the resonance structures.

Level-specific recombination cross sections, $\sigma_{RC}(i)$, into various bound levels $i \equiv n$ (SLJ) of the recombined (e + ion) system, are obtained from *partial* photoionization cross sections $\sigma_{PI}(i, g)$ of the level i into the ground level g of the recombining ion. These detailed photo-recombination cross sections are calculated in the energy region from the threshold energy up to $E(\nu = \nu_o \approx 10.0)$, where ν is the effective quantum number relative to the target level of the recombining ion. The resonances up to $\nu \leq \nu_o$ are delineated with a fine energy mesh. The electrons in this energy range generally recombine to a large number of final (e + ion) levels. The level specific rates are obtained for energies going up to infinity. Recombination cross sections are computed for all coupled symmetries and levels, and summed to obtain the total σ_{RC} using the program, RECXS (Nahar et al. 2000).

The program RECXS sums up the level specific rates for the total recombination rates, which also includes the contributions from the resonant high- n DR of $\nu_o < \nu < \infty$. As an additional check on the numerical calculations, the total recombination rate coefficients, α_R , are also calculated from the total recombination collision strength, Ω_{RC} , obtained from all the photoionization cross sections, and the high- n DR collision strengths. The agreement between the two numerical approaches is within a few percent.

The small background (non-resonant) contribution from the high- n states ($10 < n \leq \infty$) to total recombination is included as the “top-up” part, computed in the hydrogenic approximation (Nahar 1996). This contribution is important at low temperatures as the recombination rate is dominated by the RR, but negligible at high temperatures.

4. RESULTS AND DISCUSSION

The inverse processes of photoionization and recombination of $(\text{Ni XXVI} + h\nu \leftrightarrow \text{Ni XXVII} + e)$, and $(\text{Ni XXVII} + h\nu \leftrightarrow \text{Ni XXVIII} + e)$ are studied in detail. Total recombination rate coefficients for the hydrogenic Ni XXVIII are also presented alongwith those of Ni XXVI and Ni XXVII in Table 3 for completeness.

Both the total and the partial photoionization cross sections, including the autoionizing resonances, are obtained for Ni XXVI and Ni XXVII for the first time and are available electronically. The *total* photoionization cross sections correspond to leaving the core ion in various excited states and are needed in astrophysical applications, such as in ionization balance calculations. The *partial* cross sections for leaving the core in the ground level are needed for applications such as for recombination rate coefficients.

The total unified recombination collision strengths (Ω_{RC}), cross sections (σ_{RC}), and recombination rate ($\alpha_{RC}(E)$) with electron energies are presented for Ni XXVI and Ni XXVII, and data are available electronically. Total unified recombination rate coefficient, $\alpha_{RC}(T)$, are computed in two different ways to enable numerical checks: (i) from the sum of the level-specific rate coefficients and the high-n DR contribution, and (ii) from total collision strengths calculated from photoionization cross sections directly, and the DR contribution. The differences between the two are typically within a few percent, thus providing a numerical and self-consistency check particularly on the resolution of resonances.

Level-specific and total recombination rate coefficients, α_i (n SLJ, $n \leq 10$) and $\alpha_{RC}(T)$ respectively, are obtained using the BPRM unified treatment for Ni XXVI and Ni XXVII. Calculations of the recombination-cascade contributions for important lines require accurate atomic parameters for fine structure levels up to fairly high n levels, as reported here. Level-specific recombination rate coefficients of all bound levels and the summed total recombination rate coefficients ($\alpha_R(T)$) for recombined into infinite number of bound states are presented. The level-specific rate coefficients are obtained for the first time. Existing data are available only for individual total RR and DR rates.

Important features in photoionization and electron-ion recombination for each ion are discussed separately below.

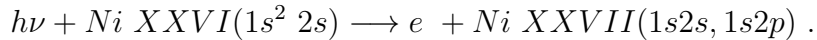
4.1. Ni XXVI

A total of 98 bound levels are found for Ni XXVI with $n \leq 10$, $0 \leq l \leq 9$, $0 \leq L \leq 11$, and total angular momentum of $1/2 \leq J \leq 17/2$ (Nahar 2002).

4.1.1. Photoionization

Cross sections (σ_{PI}) for both *total* and *partial* photoionization are obtained for all 98 bound levels of Ni XXVI.

Figs. 1(a) and (b) present the ground state photoionization cross section for Ni XXVI ($1s^2 2s\ 2S_{1/2}$). The top panel (a) presents the *total* photoionization cross section summed over the various target thresholds for ionization, and the bottom panel (b) presents the *partial* cross sections of the ground level into the ground $1s^2(1S_0)$ level of residual ion Ni XXVII. The resonances at high energies belong to the Rydberg series converging on to the $n = 2, 3$ levels of core Ni XXVII. These are the well known KLL, KLN resonances, for example, as discussed by Nahar et al. (2003). Since the first excited levels of $n=2$ thresholds of the core ion Ni XXVII lie at high energies, the cross sections decrease monotonically over a large energy range before the Rydberg series of resonances appear. The *total* and the *partial* cross sections are identical below the first excited level of the residual ion beyond which total σ_{PI} increases due to added contributions from excited channels (Fig. 1). The distinct difference between the total and partial cross sections Fig. 1 comes from the contribution of channels with excited $n=2$ thresholds. The K-shell ionization jump at the $n = 2$ target levels in total σ_{PI} is due to inner-shell photoionization:



In X-ray photoionization models inner-shell edges play an important role in overall ionization rates.

Fig. 2 presents partial photoionization cross sections of excited Rydberg series of levels $1s^2np(^2P_{1/2}^o)$, with $2 \leq n \leq 7$, of Ni XXVI. The figure illustrates the resonant structures at higher energies, especially the photoexcitation-of-core (PEC) resonances at energies associated with dipole transitions in the core ion. PEC resonances in photoionization cross sections are seen in all excited bound levels of Ni XXVI, as in Fig. 2, at photon energies 570.79, 573.67, 674.15, and 674.98 Ry due to core excitations to levels $1s2p(^3P_1^o)$, $1s2p(^1P_1^o)$, $1s3p(^3P_1^o)$, and $1s3p(^1P_1^o)$ of Ni XXVII. At these energies the core ion goes through an allowed transition, while the outer electron remains as a ‘spectator’ in a doubly-excited resonance state, followed by autoionization into the ground level of the core. The effect is more prominent for cross sections of higher excited levels. These resonances depict the non-hydrogenic behavior of cross sections of excited levels and contribute to features in level-specific recombination rates.

4.1.2. Electron-ion Recombination

The collision strength for electron-ion recombination, Ω_{RC} , is related to recombination cross sections, σ_{RC} (Eq. (10)), and show similar features. However, σ_{RC} blows up at zero electron energy. Hence the total unified photorecombination collision strength, Ω_{RC} , for Ni XXVI is presented in Fig. 3(a). Ω_{RC} , similar to photoionization cross sections σ_{PI} , decays smoothly with energy, before the emergence of resonance complexes at high energies. However, Ω_{RC} is more complex than single level σ_{PI} as it is obtained from summed contributions of σ_{PI} of all levels. The resonance complexes in Ω_{RC} (marked in the figure) are KLL, KLM, KLN etc. going up to the $n = 2$ threshold and KMM, KMN etc. going up to the $n = 3$ threshold, where KLL means $1s2l2l$, KLM means $1s2l3l'$ etc. These resonances manifest themselves as di-electronic satellite lines observed in tokamaks, Electron-Beam-Ion-Traps (EBIT), ion storage rings and astrophysical sources. The KLL complexes have been well studied in previous works (e.g. Gabriel 1972, Pradhan and Zhang 1997, Zhang et al. 1999, Oelgoetz and Pradhan 2001), for various ions.

Photorecombination rates in terms of photoelectron energy,

$$\alpha_{RC}(E) = v\sigma_{RC}(E), \quad (13)$$

where v is the photoelectron energy, an experimentally measurable quantity. Fig. 3(b) presents the expanded part of the resonances up to $n = 2$ threshold in $\alpha_{RC}(E)$ of Ni XXVI. The observed shape corresponds to the detailed $\alpha_{RC}(E)$ convolved by the monochromatic bandwidth of the experiment (e.g. for C III by Pradhan et al. 2001).

Level-specific recombination rate coefficients $\alpha_R(T)$ of 98 levels are presented for Ni XXVI. They correspond to all associated $J\pi$ levels $i \equiv n(SLJ)$ with $n \leq 10$ and $\ell \leq 9$. Fig. 4 presents $\alpha_i(T)$ into the eight lowest excited $n = 2$ and 3 levels of n (SLJ): $2s\ ^2S_0$, $2p\ ^2P_{1/2,3/2}^o$, $3s\ ^2S_0$, $3p\ ^2P_{1/2,3/2}^o$, and $3d\ ^2D_{3/2,5/2}$. These rates are relatively smooth except for a small and diffuse DR ‘bump’ at high temperature.

Total recombination rates are given in Table 3. The main features are illustrated and compared with previously available data for RR and DR rates in Fig. 5. The solid curve in the figure is the BPRM total unified $\alpha_R(T)$ and shows typical features. Starting with a higher rate coefficient at very low temperature, due to the dominance of RR into an infinity of high- n levels. $\alpha_R(T)$ decreases with increasing T until at high temperatures where it rises due to the dominance of DR, followed by a monotonic decay.

The present total unified recombination rate coefficients, $\alpha_R(T)$, for Ni XXVI are compared with RR rate coefficients (dash) by Verner and Ferland (1996), DR rates (dotted) by Jacobs et al (1980) and DR rates (chain dash) by Romanik (1988). Present rates agree very

well with the previously calculated rates, especially with the sum of RR+DR (dot-dash) of Verner and Ferland and of Jacobs et al.

4.2. Ni XXVII

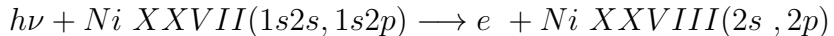
A total of 198 bound levels are found for Ni XXVII with $n \leq 10$, $0 \leq l \leq 9$, $0 \leq L \leq 14$, and total angular momentum of $0 \leq J \leq 10$.

4.2.1. Photoionization

Partial and total photoionization cross sections are presented for all 198 bound levels ($n \leq 10$) of Ni XXVII. Illustrative results are presented in Fig. 6 and 7.

Fig. 6 presents samples of level-specific photoionization cross section of Ni XXVII. The ground $1s^2 ({}^1S_0)$ level cross sections are in the topmost panel while the lower four panels present σ_{PI} of the four lowest $n = 2$ excited levels of Ni XXVII. These excited levels correspond to the prominent lines of K α complex in the X-ray emission of He-like ions; resonance (w: $1s^2 ({}^1S_0) \leftarrow 1s2p({}^1P_1^o)$), intercombination (y: $1s^2 ({}^1S_0) \leftarrow 1s2p({}^3P_1^o)$), and forbidden (x: $1s^2 ({}^1S_0) \leftarrow 1s2p({}^3P_2^o)$, and z: $1s^2 ({}^1S_0) \leftarrow 1s2s({}^3S_1)$) lines. respectively, and yield valuable spectral diagnostics of temperature, density, ionization balance, and abundances in the plasma source.

In the photoionization cross section of the ground level ($1s^2 {}^1S_0$) of Ni XXVII, the Rydberg series of resonances, KL and Kn ($n > 2$), begin at fairly high energies owing to the high $n = 2$ excitation thresholds of Ni XXVIII. However, the ground level σ_{PI} of Ni XXVII does not show a significant K-shell jump at $n = 2$ threshold, as seen in Ni XXVI. Nonetheless the K-shell ionization jump at the $n = 2$ target levels



can be seen clearly in the photoionization cross sections in Figs. 6(b)-(e).

Fig. 7 presents partial photoionization cross sections of the Rydberg series of $J = 0$ levels, $1sns({}^1S_0)$ where $2 \leq n \leq 7$, of Ni XXVII ionizing into the ground level $1s({}^2S_{1/2})$ of the core. The figure displays the PEC resonances at about 594, 704, 743 Ry (marked by arrows in the top panel) due to core transitions to allowed levels. The energy positions correspond to core levels ${}^2P_{1/2}^o, {}^2P_{3/2}^o$ of configurations $2p$, $3P$, and $4p$.

4.2.2. Electron-ion recombination

The total unified photorecombination collision strength Ω_{RC} for Ni XXVII is presented in Fig. 8(a). It corresponds to summed contributions from photoionization cross sections of all levels and high- n DR. Ω_{RC} decays smoothly with energy until resonance complexes appear at very high energy, as expected for a He-like ion. The resonance complexes are LL, LM, LN etc. going up to the $n = 2$ threshold and MM, MN etc. going up to the $n = 3$ threshold, and NN, NO etc. going up to the $n = 4$ threshold; LL means $2l2l$, LM means $2l3l'$ etc. The $n = 4$ resonances are too weak for any significant contributions.

Fig. 8(b) presents an expanded part of the resonances up to the $n = 2$ threshold of photorecombination rates ($\alpha_{RC}(E)$) varying with photoelectron energy. As mentioned before, $\alpha_{RC}(E)$ is a measurable quantity and the observed shape is usually convolved by the monochromatic bandwidth of the experiment.

Level-specific recombination rate coefficients are obtained for 198 levels of n (SLJ) with $0 \leq J \leq 10$ and $n \leq 10$. Fig. 9 presents level specific rates for the ground and the $n = 2$ levels corresponding to the X-ray w, x, y, and z lines of Ni XXVII. The rates show a relatively smooth decrease with temperature.

The total unified recombination rate coefficients are given in Table 3. The main features are illustrated and compared with previously available data for RR and DR rates in Fig. 10. The BPRM total unified $\alpha_R(T)$ (solid curve in the figure) shows typical features. The high recombination rate coefficients at very low temperature, due to the dominance of RR into an infinity of high- n levels, decreases with increasing T until at high temperatures where it shows a "shoulder" due to the dominance of DR, which is followed by a monotonic decay.

The present total unified recombination rate coefficients, $\alpha_R(T)$, for Ni XXVI are compared with RR rate coefficients (dash) by Verner and Ferland (1996) and DR rates (dotted) by Jacobs et al (1980). Present rates agree very well with the previously calculated rates, especially with the sum of RR+DR (dot-dash) of Verner and Ferland and of Jacobs et al.

5. CONCLUSION

Extensive results from relativistic calculations for total and level-specific photoionization and recombination cross sections and rates are presented for Ni XXVI and Ni XXVII. These are of general interest in UV and X-ray spectroscopy of laboratory and astrophysical sources.

The present level-specific data can be used to construct recombination-cascade matrices for Ni XXVI and Ni XXVII to obtain effective recombination rates into specific fine structure

levels n (SLJ) with $n \leq 10$ and $\ell \leq n - 1$ (e.g. Pradhan 1985). Present total unified recombination rates agree very well with the sum of RR and DR of previous calculations. It is expected for the He- and Li-like ions for which electron-electron correlation is weak resulting in a small interference between RR and DR. However, the unified method for recombination provides level-specific rates of hundreds of levels and corresponding self-consistent photoionization cross sections of many bound levels, not obtainable by other existing methods. The present data is more than sufficient for extrapolation to high- n, ℓ necessary to account for all cascade contributions.

The available data includes: (i) Photoionization cross sections, both total and partial, for bound fine structure levels of Ni XXVI and Ni XXVII up to the $n = 10$ levels. (ii) Total unified recombination rate coefficients for Ni XXVI and Ni XXVII, and level-specific recombination rate coefficients for levels up to $n = 10$, (iii) total unified recombination collision strength, cross sections and rates with photoelectron energies of Ni XXVI and Ni XXVII. Further calculations for other He-like and Li-like ions are in progress. All photoionization and recombination data are available electronically at: nahar@astronomy.ohio-state.edu.

This work was supported partially by NSF and NASA. The computational work was carried out on the Cray SV1 at the Ohio Supercomputer Center in Columbus, Ohio.

Table 1: Ion core levels in the eigenfunction expansions of Ni XXVI and Ni XXVII.

Ni XXVII		Ni XXVIII			
level	$E_t(Ry)$	level	$E_t(Ry)$		
1	$1s^2(^1S_0)$	0.0	1	$1s(^2S_{1/2})$	0.00
2	$1s2s(^3S_1)$	568.2566	2	$2p(^2P_{1/2}^o)$	593.654
3	$1s2p(^3P_0^o)$	570.5865	3	$2s(^2S_{1/2})$	593.686
4	$1s2s(^1S_0)$	570.792	4	$2p(^2P_{3/2}^o)$	595.723
5	$1s2p(^3P_1^o)$	570.7938	5	$3p(^2P_{1/2}^o)$	704.226
6	$1s2p(^3P_2^o)$	572.2873	6	$3s(^2S_{1/2})$	704.238
7	$1s2p(^1P_1^o)$	573.6669	7	$3d(^2D_{3/2})$	704.821
8	$1s3s(^3S_1)$	673.4568	8	$3p(^2P_{3/2}^o)$	704.823
9	$1s3p(^3P_0)$	674.1039	9	$3d(^2D_{5/2})$	705.024
10	$1s3s(^1S_0)$	674.1223	10	$4p(^2P_{1/2}^o)$	742.836
11	$1s3p(^3P_1^o)$	674.1493	11	$4s(^2S_{1/2})$	742.841
12	$1s3p(^3P_2^o)$	674.5945	12	$4d(^2D_{3/2})$	743.065
13	$1s3p(^1P_1^o)$	674.9808	13	$4p(^2P_{3/2}^o)$	743.078
14	$1s3d(^3D_1)$	676.624	14	$4d(^2D_{5/2})$	743.148
15	$1s3d(^3D_2)$	676.632	15	$4f(^2F_{5/2}^o)$	743.162
16	$1s3d(^1D_3)$	676.806	16	$4f(^2F_{7/2}^o)$	743.205
17	$1s3d(^1D_2)$	676.819			

Ni XXVII: Correlations - $2s^2$, $2p^2$, $3s^2$, $3p^2$, $3d^2$, $2s2p$,
 $2s3s$, $2s3p$, $2s3d$, $2s4s$, $2s4p$, $2p3s$, $2p3p$, $2p3d$, $2p4s$, $2p4p$,

Ni XXVII: λ_{nl} - 1.0, for 1s to 4p

Ni XXVIII: No correlations; λ_{nl} - 1.0, for 1s to 4f

Table 2: Radiative decay rates, A_{ji} , in sec^{-1} for allowed transitions to the ground level, $1s^2 ^1S_0$ for Ni XXVII and $1s ^2S_{1/2}$ for Ni XXVIII (specified in the column title).

Target State	A_{fi} (s^{-1})	Target State	A_{fi} (s^{-1})
Ni XXVII: GD- $1s^2 ^1S_0$			
$1s2p(^3P_3^o)$	7.21(13)	$1s3p(^3P_3^o)$	2.17(13)
$1s2p(^3P_1^o)$	6.23(14)	$1s3p(^3P_1^o)$	1.80(14)
Ni XXVIII: GD- $1s ^2S_{1/2}$			
$2p(^2P_{1/2}^o)$	3.79(14)	$3p(^2P_{3/2}^o)$	9.73(13)
$2p(^2P_{3/2}^o)$	3.80(14)	$4p(^2P_{1/2}^o)$	3.23(13)
$3p(^2P_{1/2}^o)$	9.34(13)	$4p(^2P_{3/2}^o)$	3.50(13)

Table 3: Total recombination rate coefficients $\alpha_R(T)$ for Ni XXVI, Ni XXVII and Ni XXVIII.

$\log_{10}T$ (K)	$\alpha_R(cm^3s^{-1})$			$\log_{10}T$ (K)	$\alpha_R(cm^3s^{-1})$		
	Ni XXVI	Ni XXVII	Ni XXVIII		Ni XXVI	Ni XXVII	Ni XXVIII
1.0	2.86E-08	3.28E-08	3.72E-08	5.1	1.21E-10	1.50E-10	1.80E-10
1.1	2.54E-08	2.92E-08	3.31E-08	5.2	1.04E-10	1.29E-10	1.56E-10
1.2	2.26E-08	2.60E-08	2.95E-08	5.3	8.92E-11	1.11E-10	1.35E-10
1.3	2.01E-08	2.31E-08	2.62E-08	5.4	7.65E-11	9.61E-11	1.17E-10
1.4	1.78E-08	2.05E-08	2.33E-08	5.5	6.55E-11	8.27E-11	1.01E-10
1.5	1.58E-08	1.82E-08	2.07E-08	5.6	5.59E-11	7.12E-11	8.69E-11
1.6	1.40E-08	1.62E-08	1.84E-08	5.7	4.77E-11	6.11E-11	7.50E-11
1.7	1.24E-08	1.43E-08	1.63E-08	5.8	4.07E-11	5.24E-11	6.46E-11
1.8	1.10E-08	1.27E-08	1.44E-08	5.9	3.46E-11	4.49E-11	5.56E-11
1.9	9.74E-09	1.12E-08	1.28E-08	6.0	2.93E-11	3.84E-11	4.78E-11
2.0	8.60E-09	9.94E-09	1.13E-08	6.1	2.48E-11	3.28E-11	4.10E-11
2.1	7.60E-09	8.78E-09	1.00E-08	6.2	2.10E-11	2.80E-11	3.53E-11
2.2	6.70E-09	7.76E-09	8.85E-09	6.3	1.77E-11	2.39E-11	3.02E-11
2.3	5.90E-09	6.84E-09	7.81E-09	6.4	1.49E-11	2.03E-11	2.58E-11
2.4	5.20E-09	6.03E-09	6.89E-09	6.5	1.25E-11	1.72E-11	2.21E-11
2.5	4.58E-09	5.31E-09	6.07E-09	6.6	1.05E-11	1.46E-11	1.88E-11
2.6	4.01E-09	4.67E-09	5.35E-09	6.7	8.72E-12	1.23E-11	1.60E-11
2.7	3.52E-09	4.10E-09	4.70E-09	6.8	7.26E-12	1.04E-11	1.36E-11
2.8	3.09E-09	3.60E-09	4.14E-09	6.9	6.03E-12	8.75E-12	1.16E-11
2.9	2.71E-09	3.16E-09	3.63E-09	7.0	5.00E-12	7.35E-12	9.78E-12
3.0	2.37E-09	2.77E-09	3.19E-09	7.1	4.17E-12	6.18E-12	8.25E-12
3.1	2.07E-09	2.43E-09	2.80E-09	7.2	3.51E-12	5.22E-12	6.97E-12
3.2	1.81E-09	2.13E-09	2.45E-09	7.3	3.01E-12	4.44E-12	5.85E-12
3.3	1.58E-09	1.86E-09	2.15E-09	7.4	2.63E-12	3.82E-12	4.90E-12
3.4	1.38E-09	1.63E-09	1.88E-09	7.5	2.32E-12	3.30E-12	4.10E-12
3.5	1.21E-09	1.42E-09	1.65E-09	7.6	2.05E-12	2.86E-12	3.41E-12
3.6	1.05E-09	1.24E-09	1.44E-09	7.7	1.78E-12	2.47E-12	2.83E-12
3.7	9.14E-10	1.08E-09	1.26E-09	7.8	1.53E-12	2.10E-12	2.34E-12
3.8	7.95E-10	9.44E-10	1.10E-09	7.9	1.28E-12	1.77E-12	1.92E-12
3.9	6.91E-10	8.22E-10	9.59E-10	8.0	1.06E-12	1.46E-12	1.58E-12
4.0	6.00E-10	7.16E-10	8.37E-10	8.1	8.52E-13	1.19E-12	1.28E-12
4.1	5.21E-10	6.23E-10	7.29E-10	8.2	6.76E-13	9.60E-13	1.04E-12
4.2	4.52E-10	5.42E-10	6.37E-10	8.3	5.29E-13	7.64E-13	8.36E-13
4.3	3.92E-10	4.71E-10	5.54E-10	8.4	4.09E-13	6.01E-13	6.70E-13
4.4	3.39E-10	4.09E-10	4.82E-10	8.5	3.13E-13	4.69E-13	5.33E-13
4.5	2.94E-10	3.55E-10	4.20E-10	8.6	2.37E-13	3.64E-13	4.22E-13
4.6	2.54E-10	3.08E-10	3.65E-10	8.7	1.79E-13	2.80E-13	3.32E-13
4.7	2.19E-10	2.67E-10	3.17E-10	8.8	1.34E-13	2.14E-13	2.59E-13
4.8	1.89E-10	2.32E-10	2.76E-10	8.9	1.00E-13	1.63E-13	2.02E-13
4.9	1.63E-10	2.00E-10	2.39E-10	9.0	7.44E-14	1.24E-13	1.56E-13
5.0	1.41E-10	1.73E-10	2.08E-10				

REFERENCES

Bell, R.H. & Seaton, M.J. 1985, J. Phys. B 18, 1589

Berrington, K. A., Burke, P.G., Butler, K., Seaton, M.J., Storey, P.J., Taylor, K.T. & Yu Yan 1987, J. Phys. B 20, 6379

Berrington, K.A., Eissner, W., Norrington, P.H. 1995, Comput. Phys. Commun. 92, 290

Canizares et al. 2000, in Proceedings of the NASA workshop on *Atomic data needs in X-ray astronomy*, Eds. M.A. Bautista, T. R. Kallman, A.K. Pradhan, 2000, NASA Publications NASA/CP-2000-209968, ADXA, (<http://heasarc.gsfc.nasa.gov/docs/heasarc/atomic/proceed.html>)

Eissner, W., Jones, M., & Nussbaumer, H. 1974, Comput. Phys. Commun. 8, 270

Gabriel, A.H. 1972, Mon. Not. R. astr. Soc. 1972, 160, 99

Hummer, D.G., Berrington, K.A., Eissner, W., Pradhan, A.K., Saraph, H.E., & Tully, J.A. 1993, Astron. Astrophys. 279, 298

Jacobs, V.L., Davis, J., Rogerson, J.E., Blaha, M., Cain, J., & Davis, M. 1980, ApJ 239, 1119

Nahar, S.N. 1996, Phys. Rev. A 53, 2417

Nahar, S.N. 2002, A&A 389, 716

Nahar, S.N. & Pradhan, A.K. 1992, Phys. Rev. Lett. 68, 1488

Nahar, S.N. & Pradhan, A.K. 1994, Phys. Rev. A 49, 1816

Nahar, S.N. & Pradhan, A.K. 1997, APJS 111, 339

Nahar, S.N. & Pradhan, A.K. 2000, Phys. Scr. 61, 675

Nahar, S.N. & Pradhan, A.K. 2003, ApJS 149, 239

Nahar, S.N., Pradhan, A.K. & Zhang, H.L. 2000, ApJS 131, 375

Nahar, S.N., Pradhan, A.K. & Zhang, H.L. 2001, ApJS 133, 255

NIST compiled database, www.nist.gov

Oelgoetz, J. & Pradhan A.K. 2001, MNRAS 327, L42

Pradhan, A.K. 1985, Astrophys. J. 284, 824

Pradhan, A.K., Chen, Guo Xin, Nahar, S.N., and Zhang, H. L. 2001, Phys. Rev. Lett. 87, 183201

Pradhan, A.K. and Zhang, H. L. 1997, J. Phys. B 30, L571

Romanik, C. 1988, Astrophys. J. 330, 1022

Sakimoto K., Terao M., & Berrington K.A. 1990, Phys. Rev. A 42, 291

Scott N.S. & Burke P.G. 1980, J. Phys. B 12, 4299

Scott N.S. & Taylor K.T. 1982, Comput. Phys. Commun. 25, 347

Seaton, M.J. 1987, J. Phys. B 20, 6363

Verner, D.A. & Ferland G. 1996, ApJS, 103, 467

Zhang, H.L., Nahar, S.N. & Pradhan, A.K. 1999, J. Phys. B, 32, 1459

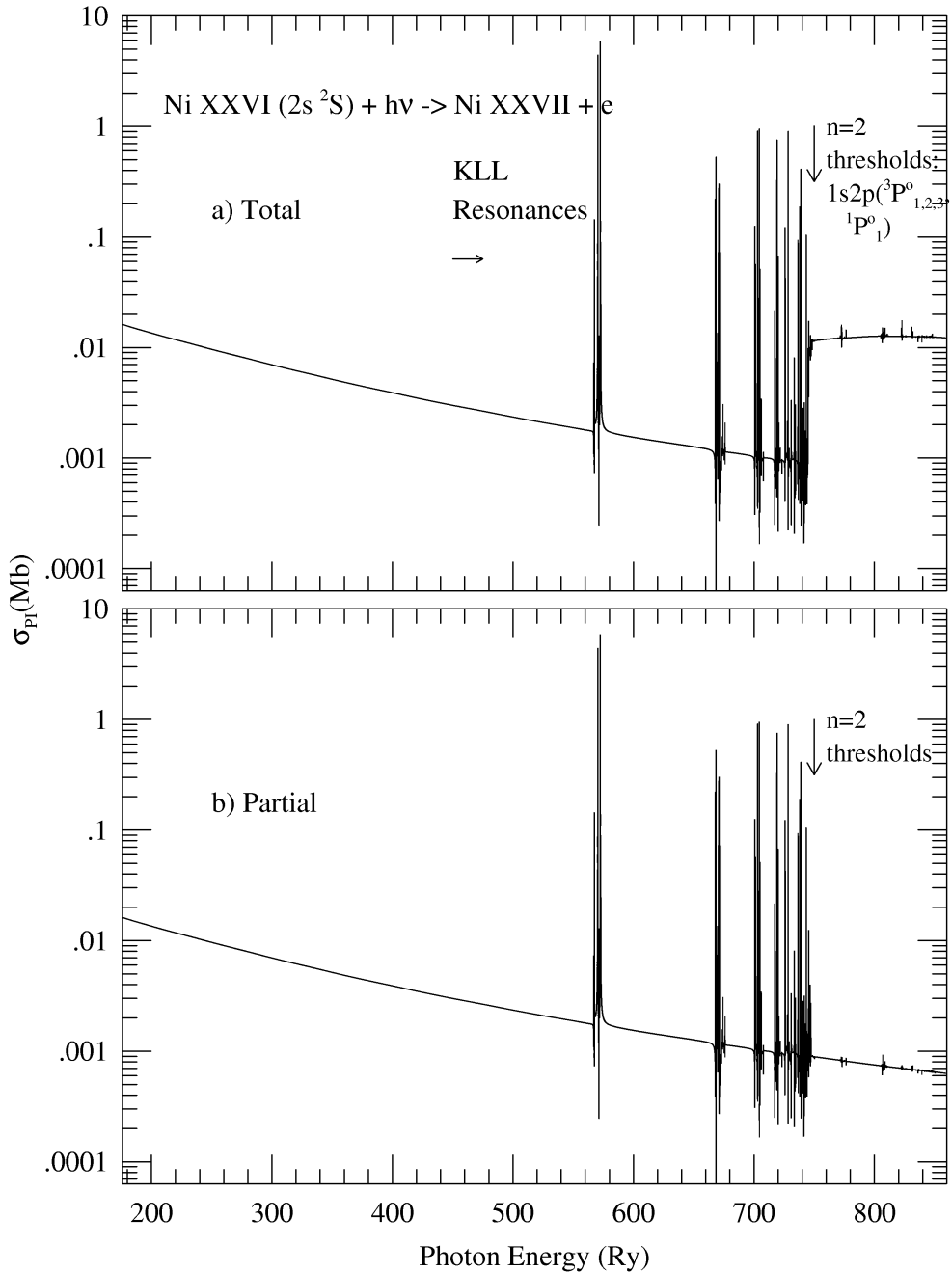


Fig. 1.— Photoionization cross sections (σ_{PI}) of the ground level $1s^2 2s$ ($^2S_{1/2}$) of Ni XXVI: (a) Total cross section; the large jump around $n = 2$ thresholds (~ 735 Ry) is the K-shell ionization edge ($h\nu + 1s^2 2l \rightarrow 1s2l + e$). (b) Partial cross section into the ground level $1s^2$ (1S_0) of Ni XXVII; note that the jump is no longer present and the cross section is continuous across the $n = 2$ thresholds of Ni XXVII.

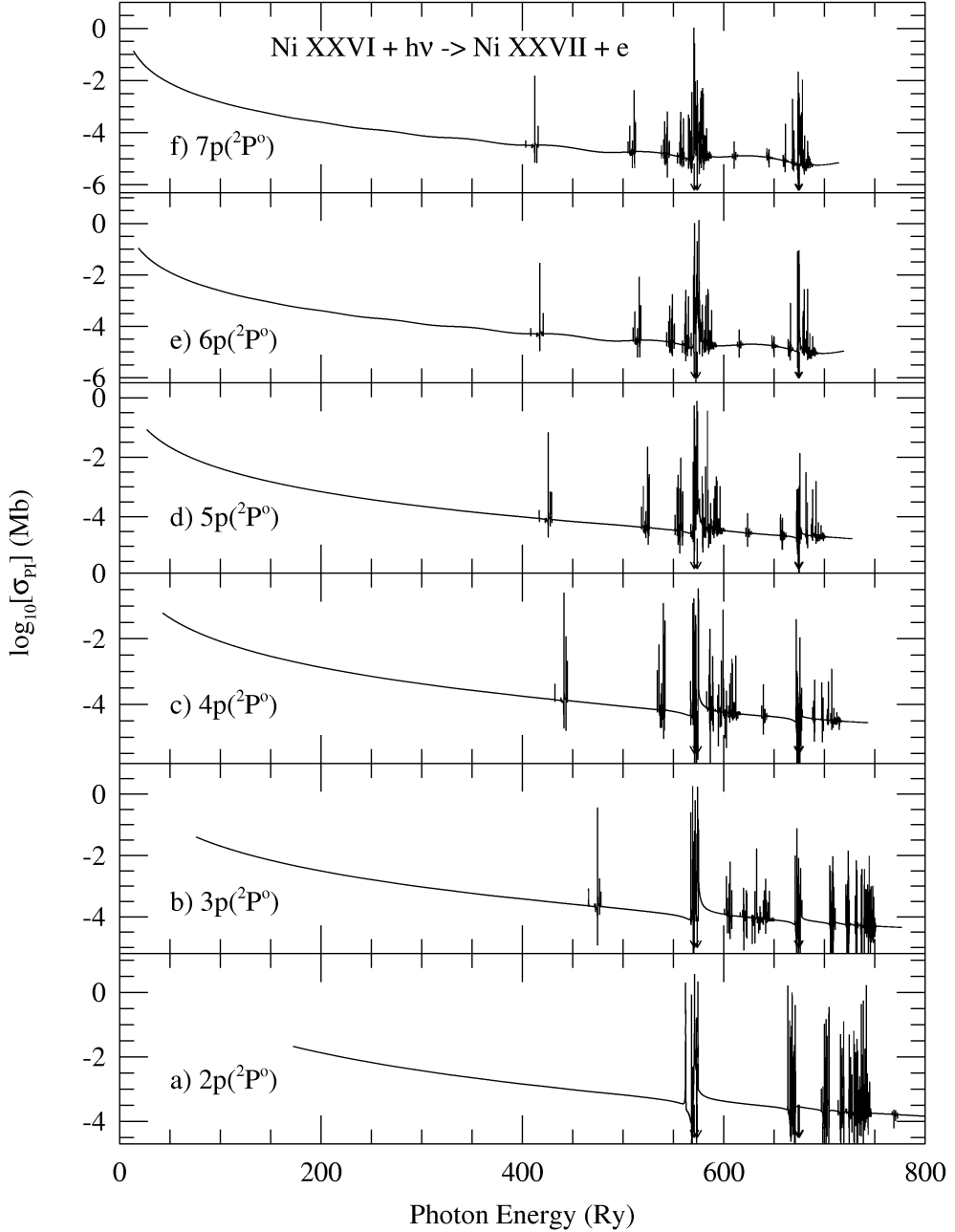


Fig. 2.— Partial photoionization cross sections of the Rydberg series of levels, $1s^2np(^2P_{1/2}^o)$ with $2 \leq n \leq 7$, of Ni XXVI into the ground level $1s^2(^1S_0)$ of Ni XXVII. Prominent PEC (*photoexcitation-of-core*) resonances are seen (pointed by arrows) at about 571 Ry of excited core levels $1s2p\ ^3P_1^o, ^1P_1^o$ and about 674 Ry of levels $1s3p\ ^3P_1^o, ^1P_1^o$.

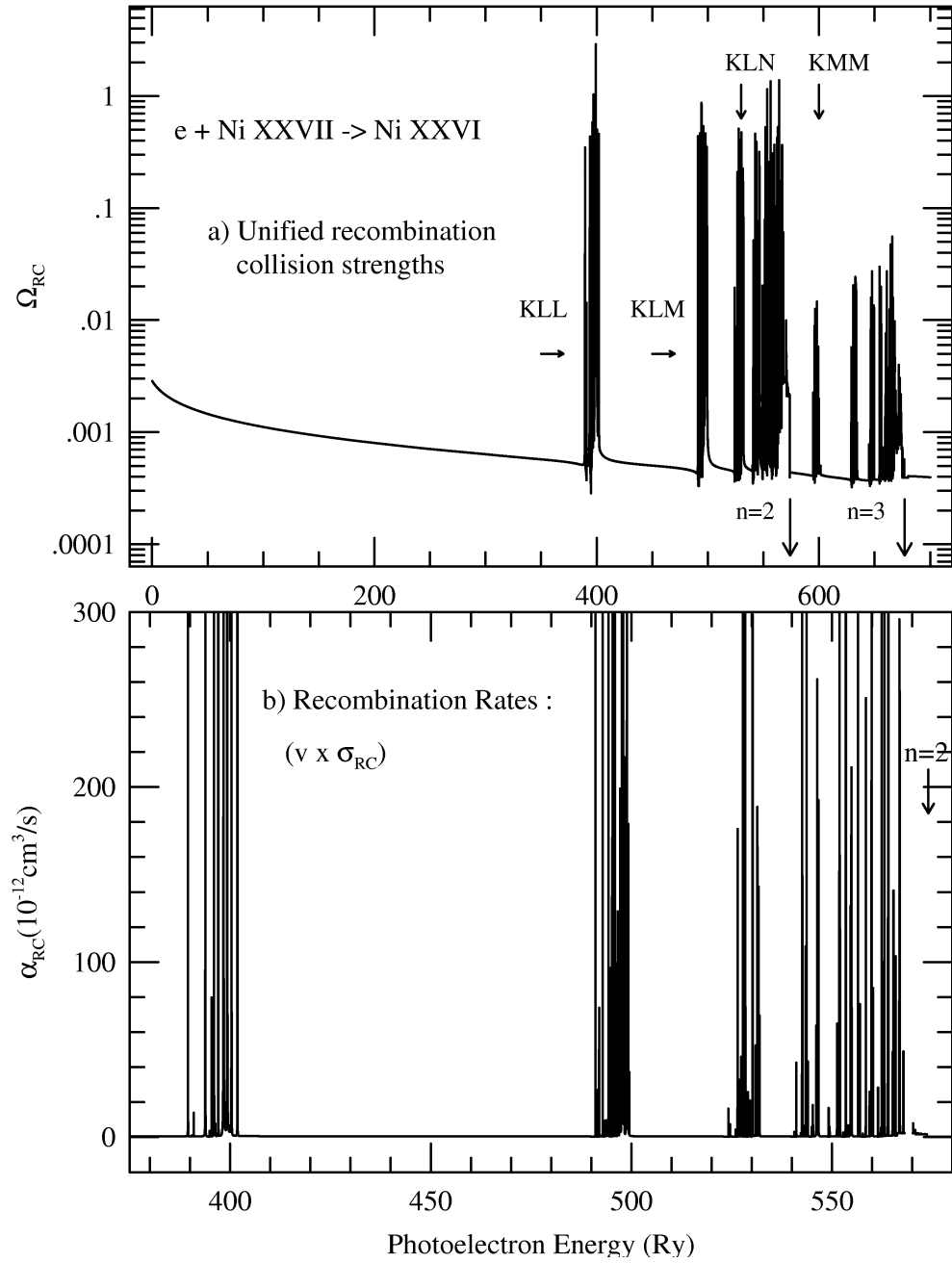


Fig. 3.— (a) Total unified ($e + \text{ion}$) recombination collision strengths, Ω_{RC} and (b) unified recombination rate coefficients, $\alpha_{RC}(E)$, with photoelectron energy of Ni XXVI. Note separated resonance complexes, KLL, KLM, etc of $n = 2$ and KMM, KMN etc. of $n = 3$ thresholds. $\alpha_{RC}(E)$, convolved with a bandwidth is a measurable quantity.

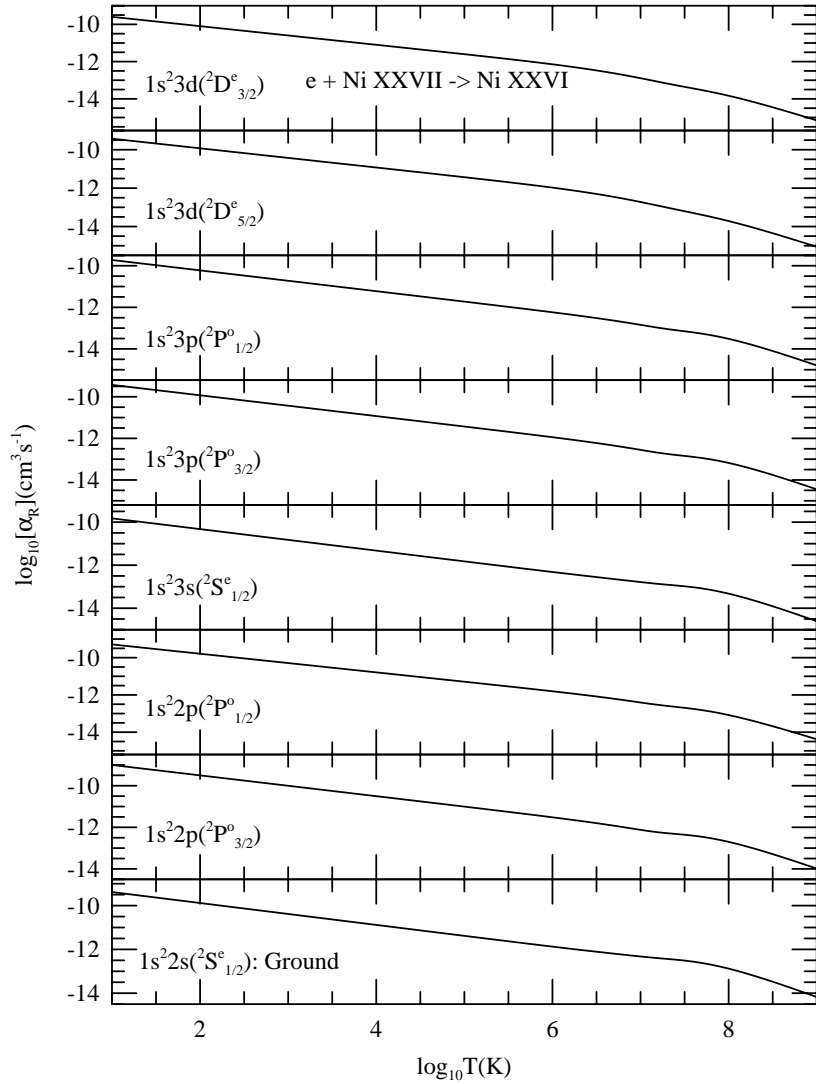


Fig. 4.— Level-specific recombination rate coefficients for Ni XXVI recombining to ground and excited $n=2, 3$ levels.

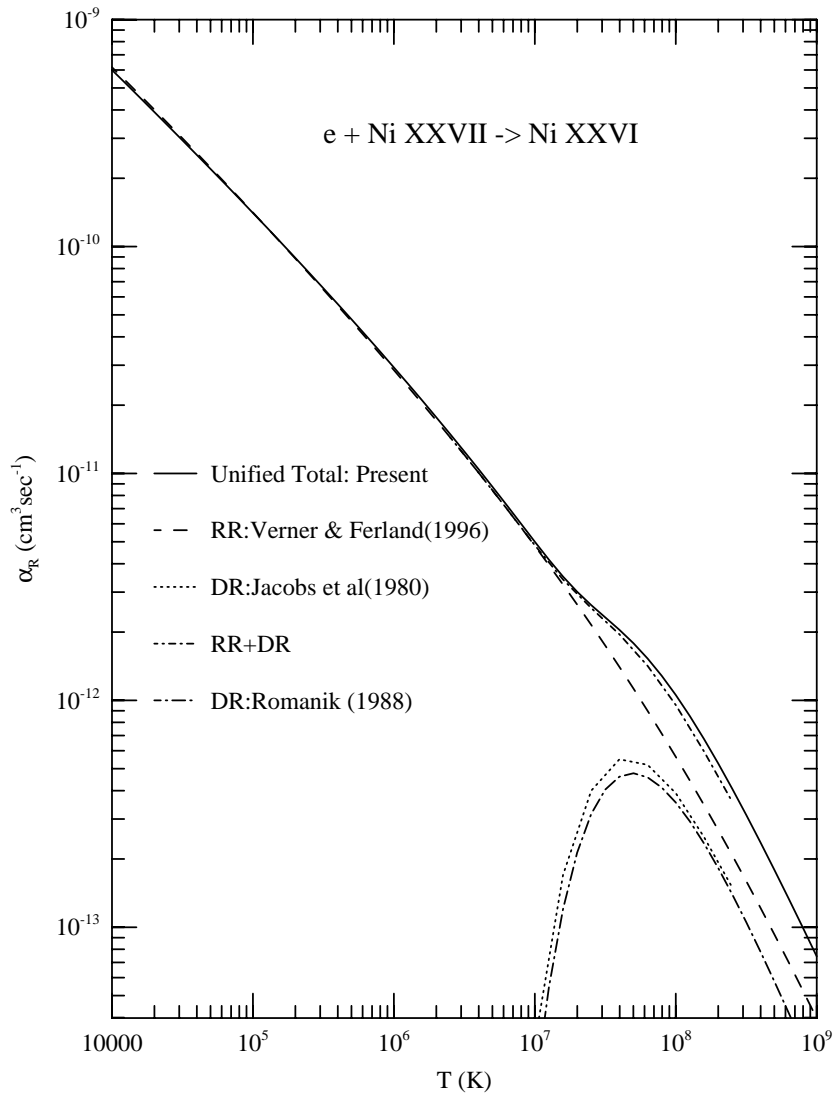


Fig. 5.— Total unified recombination rate coefficients, $\alpha_R(T)$, for Ni XXVI: total unified (solid curve), RR rates (dash) by Verner and Ferland (1996), DR rates (dotted) by Jacobs et al (1980) and DR rates (chain dash) by Romanik (1988), and sum of RR+DR (dot-dash).

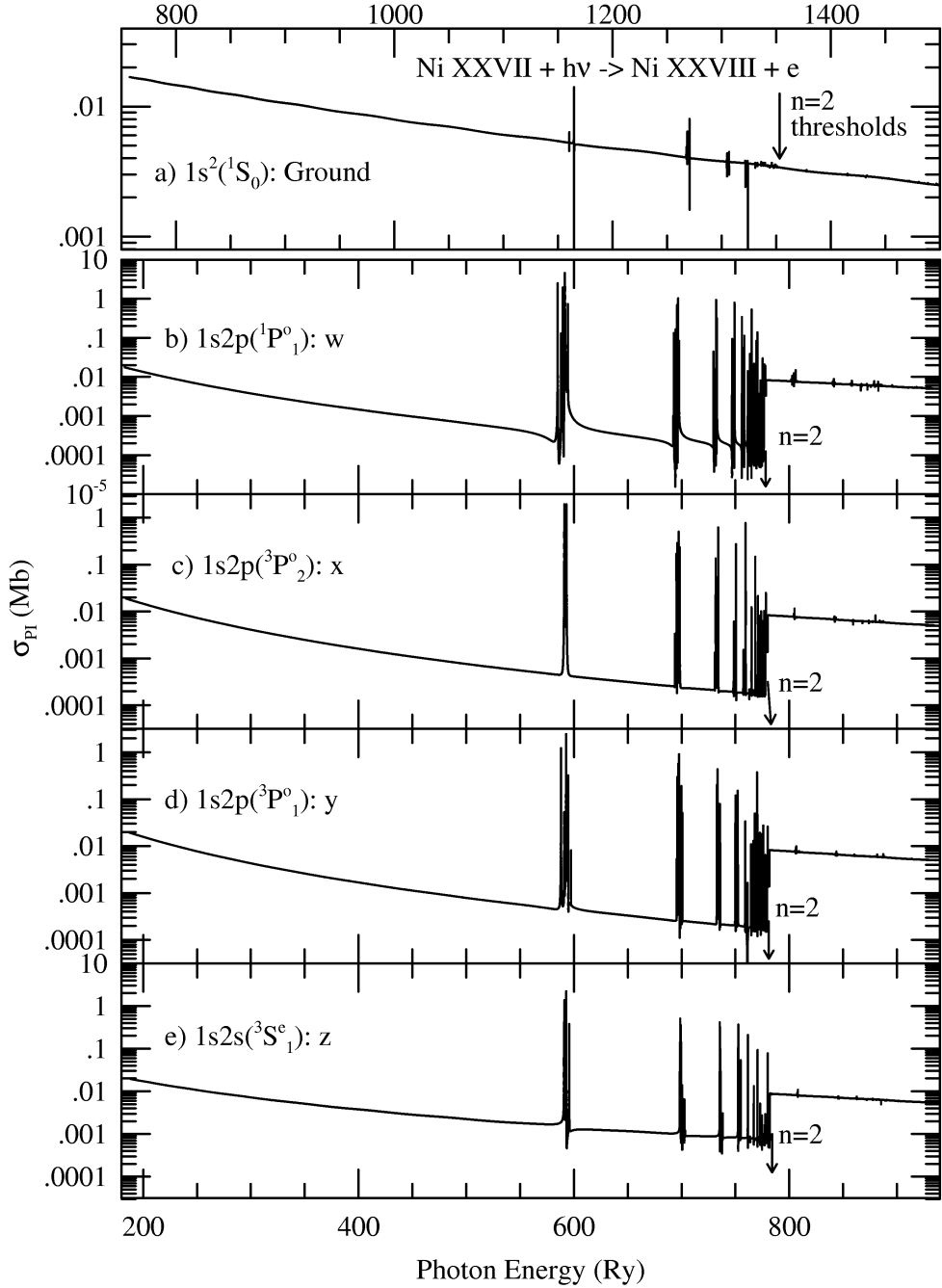


Fig. 6.— Level-specific photoionization cross sections of (a) the ground $1s^2$ (1S_0), and excited (b) $1s2p(^1P_1)$ -w, (c) $1s2p(^3P_2)$ -x, (d) $1s2p(^3P_1)$ -y, (e) $1s2s(^3S_1)$ -z levels of Ni XXVII. The excited levels correspond to the prominent X-ray lines: resonance (w), intercombination (y), and forbidden(x,z) and show K-shell ionization edge at $n = 2$ thresholds.

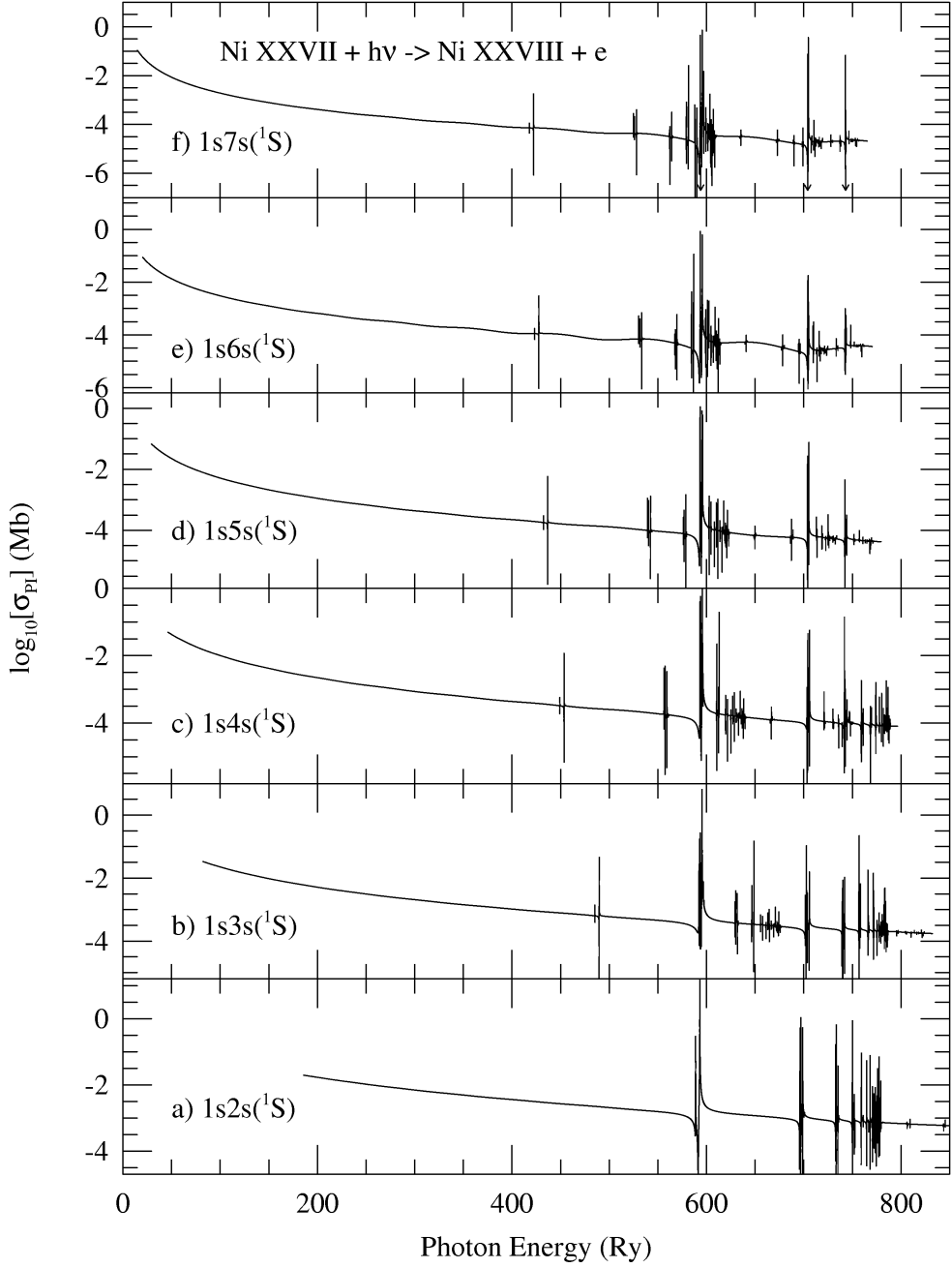


Fig. 7.— Partial photoionization cross sections of the Rydberg series of levels $1sns(^1S_0)$, $2 \leq n \leq 7$, of Ni XXVII into the ground level $1s(^2S_{1/2})$ of the core, displaying PEC (*photoexcitation-of-core*) resonances at about 594, 704, 743 Ry (marked by arrows in the top panel) of core levels $^2P_{1/2,3/2}^o$ of configurations $2p$, $3P$, and $4p$.

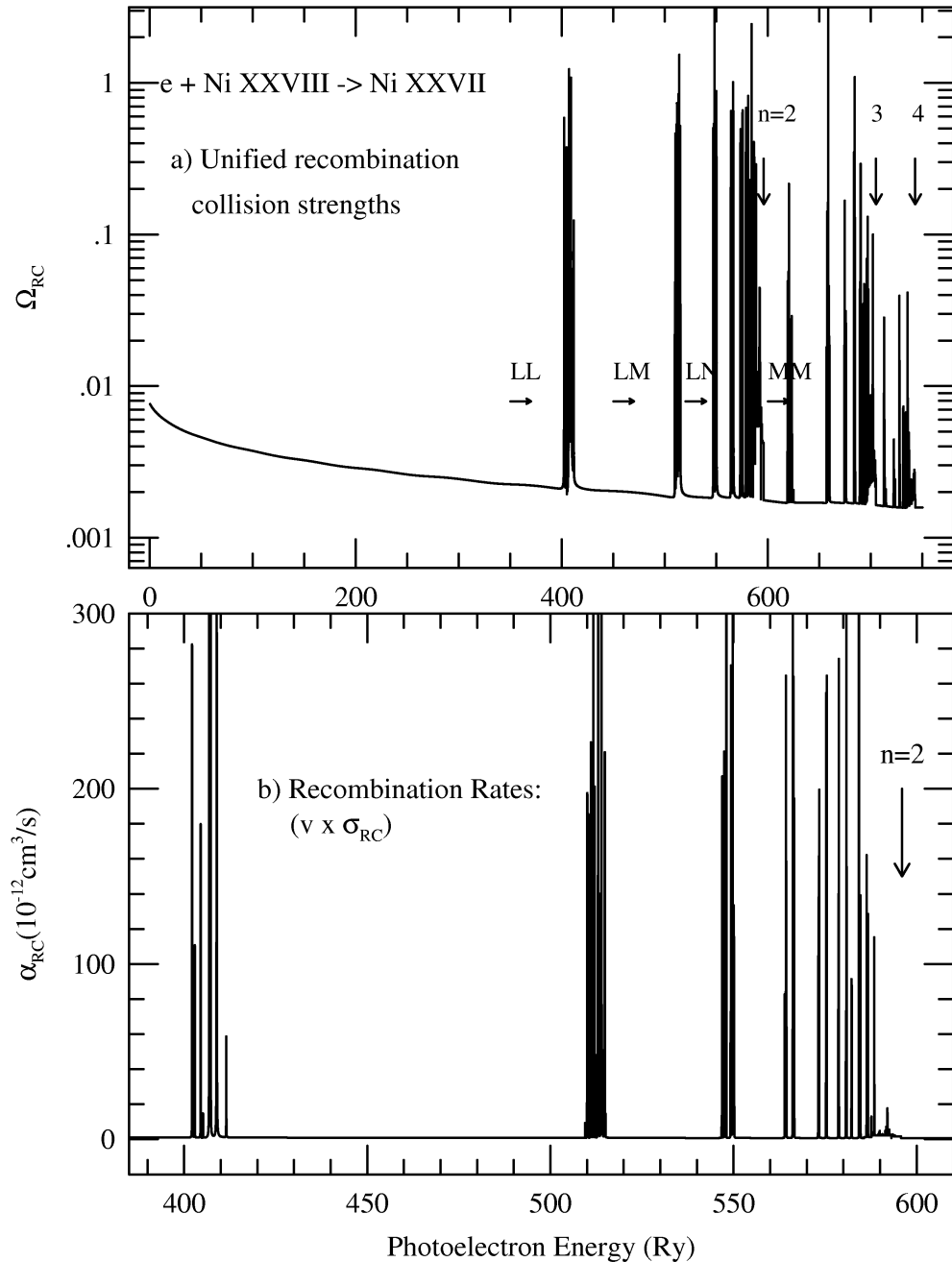


Fig. 8.— (a) Total unified (e + ion) recombination collision strengths, Ω_{RC} and (b) unified recombination rate coefficients, $\alpha_{RC}(E)$ with photoelectron energy of Ni XXVII. Note the separated resonance complexes, LL, LM, etc of $n = 2$ and MM, MN etc. of $n = 3$ and NN, NO etc of $n = 4$ thresholds. $\alpha_{RC}(E)$, convolved with a bandwidth, is a measurable quantity.

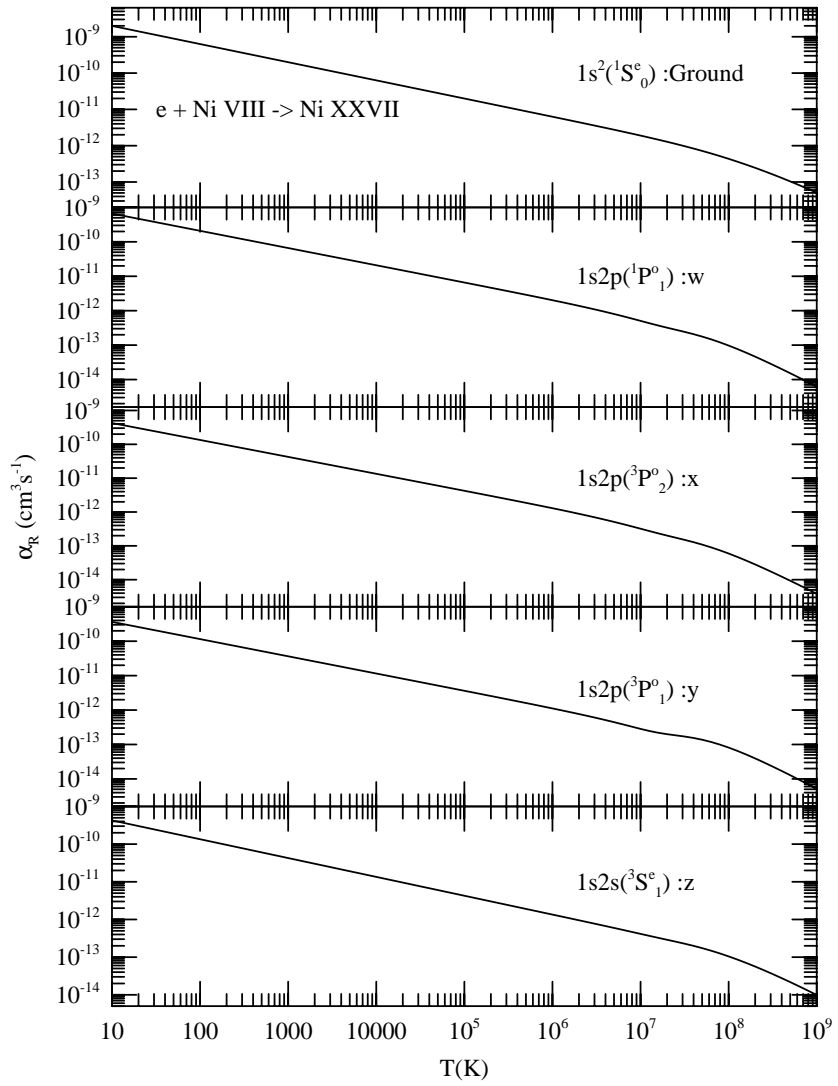


Fig. 9.— Level-specific recombination rate coefficients for Ni XXVII into the ground and excited $n = 2$ levels responsible for the prominent X-ray w, x, y, and z lines.

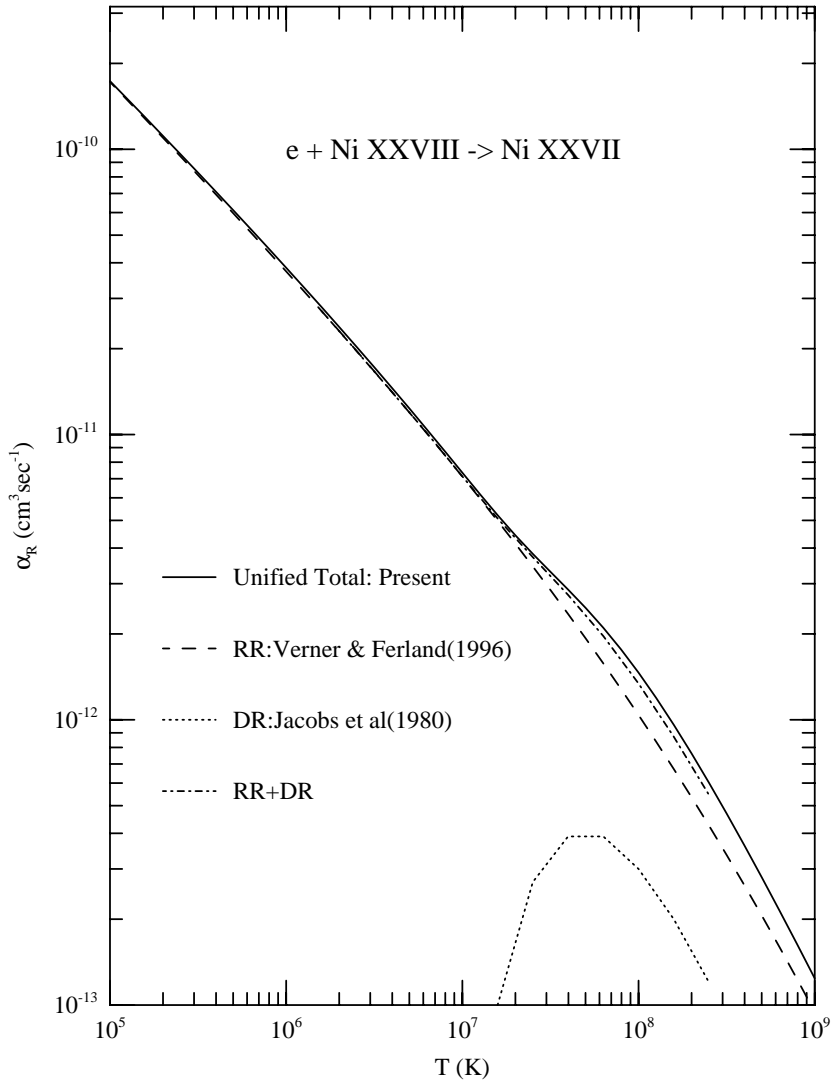


Fig. 10.— Total unified recombination rate coefficients, $\alpha_R(T)$, for Ni XXVII: present unified total (solid), RR rates (dash) by Verner and Ferland (1996), DR rates (dot) by Jacobs et al. (1980).